Title

Volumetric voxelwise apparent diffusion coefficient histogram analysis for differentiation of the fourth ventricular tumors.

Journal

The neuroradiology journal, 31(6)

ISSN

1971-4009

Authors

Payabvash, Seyedmehdi
Tihan, Tarik
Cha, Soonmee

Publication Date

2018-12-01

DOI

10.1177/1971400918800803

Peer reviewed

Differentiation of Cerebellar Hemisphere Tumors: Combining Apparent Diffusion Coefficient Histogram Analysis and Structural MRI Features

Seyedmehdi Payabvash, Tarik Tihan, Soonmee Cha

From the Department of Radiology and Biomedical Imaging, Yale School of Medicine, New Haven, CT (SP); Department of Radiology and Biomedical Imaging, University of California, San Francisco, CA (SP, SC); and Department of Pathology, University of California, San Francisco, CA (TT).

ABSTRACT

BACKGROUND AND PURPOSE: **We aimed to develop a diagnostic algorithm for differentiation of cerebellar hemisphere tumors, combining Apparent Diffusion Coefficient (ADC) histogram analysis and structural imaging features.**

METHODS: **Pretreatment MRI of patients with pathologically proven cerebellar hemisphere neoplasms were reviewed. Voxel-wise volumetric ADC histograms of tumor solid components were determined. Histogram variables, patients' age, and structural imaging features were applied to develop a differential diagnosis algorithm.**

RESULTS: **Among 142 patients, the most common tumors were metastasis ($n = 54$), hemangioblastoma ($n = 39$), pilocytic astrocytoma ($n = 18$), and medulloblastoma ($n = 9$). On ADC histogram analysis, medulloblastomas had the lowest, and pilocytic astrocytomas had the highest ADC values. An ADC 15th percentile value $< 580 \times 10^{-6}$ mm^2/s could differentiate medulloblastomas from other cerebellar hemisphere tumors with receiver operating characteristic (ROC) area under the curve (AUC) of .98 ($P < .001$). Comparing the two most common adult cerebellar hemisphere tumors (metastases and hemangioblastomas), hemangioblastomas had higher ADC values; and an ADC 90th percentile value $> 2000 \times 10^{-6}$ mm^2/s could identify hemangioblastomas with ROC AUC of .82 ($P < .001$). Along with ADC histogram and patients' age, structural imaging features including enhancement pattern, prominent vascular flow voids, surrounding FLAIR hyperintensity, and solid component T2 signal hyperintensity were independent differentiation variables in the diagnostic algorithm.**

CONCLUSION: **In pretreatment differentiation of cerebellar tumors, the ADC histogram analysis is particularly helpful for distinction of medulloblastomas from other subtypes, and differentiation of the two most common adult tumors (ie, metastases and hemangioblastomas) from each other. Combination of structural imaging features and ADC histogram analysis can help with pretreatment differentiation of cerebellar tumors.**

Keywords: cerebellar hemisphere, brain neoplasms, diffusion imaging, histogram analysis, differential diagnosis algorithm.

Acceptance: Received June 10, 2018, and in revised form July 7, 2018. Accepted for publication July 10, 2018.

Correspondence: Address correspondence to Soonmee Cha, MD, Department of Radiology and Biomedical Imaging, University of California, San Francisco, 350 Parnassus Avenue, Box 0336, San Francisco, CA. E-mail: Soonmee.Cha@ucsf.edu

Acknowledgements and Disclosure: No external source of funding. The authors have no competing interest related to the study. The authors thank Ms. Pari Kamal for editorial assistance and critical review of the manuscript.

J Neuroimaging 2018;28:656-665.
DOI: 10.1111/jon.12550

Introduction

The posterior cranial fossa is the most common location for pediatric brain tumors,[1] which are predominantly located in or close to the midline, and comprised primarily of medulloblastoma, ependymoma, and pilocytic astrocytoma.[2] In adults, however, posterior fossa tumors are often located off-midline in cerebellar hemispheres.[1] Differentiation of cerebellar hemisphere tumors, based on pretreatment MRI, may pose a diagnostic dilemma for neuroradiologists.

Metastases and hemangioblastomas are the two most common and important differential diagnoses of cerebellar masses in adult population. While hemangioblastomas are characterized by marked vascularity and avid enhancement,[3] metastases may have various imaging presentations based on their primary origin. Also, many pilocytic astrocytomas–classically described as cystic tumors with mural modularity–localize to cerebellar hemisphere, particularly those without gangliocytic differentiation.[4] Medulloblastomas characteristically present as midline masses along the 4th ventricle roof in pediatric patients; whereas, cerebellar hemisphere medulloblastomas typically belong to the sonic hedgehog molecular subtype and are commonly seen in adults.[5,6] On the other hand, infratentorial ependymomas tend to present as 4th ventricle floor lesions extending through the foramina of Luschka and Magendie.[1,7,8] Published studies suggest that diffusion-weighted imaging (DWI) characteristics of these tumors may help with pretreatment differentiation.[1,7,8]

The DWI and Apparent Diffusion Coefficient (ADC) maps have shown potential for pretreatment differentiation of various brain neoplasms.[9–11] The ADC values represent alterations in water diffusion, and reflect variable degrees of tissue cellularity and integrity of cell membranes.[1] In brain tumors, lower ADC values correlate with higher cell density and tumor grade.[12] Recently, ADC histogram analysis of brain tumors has shown to provide quantitative physiologic data in addition to standard MRI sequences for differentiation and grading of brain

Table 1. Surgical Pathology Diagnosis of Cerebellar Hemisphere Tumors ($n = 142$)

Diagnosis	Patients Number (Frequency)
Metastasis	54 (38.0%)
Hemangioblastoma	39 (27.5%)
Pilocytic astrocytoma	18 (12.7%)
Medulloblastoma	9 (6.3%)
Lymphoma	6 (4.2%)
Low grade glioma/astrocytoma	5 (3.5%)
Glioblastoma multiforme	4 (2.8%)
Ependymoma	2 (1.4%)
Atypical teratoid/rhabdoid tumor	2 (1.4%)
Anaplastic astrocytoma	1 (.7%)
Ganglioglioma	1 (.7%)
Anaplastic pleomorphic xanthoastrocytoma	1 (.7%)

tumors.[8,12,13] For example, the tumor ADC histogram variables correlate with survival in patients with diffuse pontine glioma and glioblastoma multiforme (GBM).[13,14] The ADC histogram variables were also helpful in the differentiation of pediatric posterior cranial fossa tumors.[9]

The purpose of our study was to apply ADC histogram analysis along with other structural imaging features for pretreatment diagnostic differentiation of cerebellar hemisphere tumors. While many prior studies have evaluated limited ADC histogram variables (eg, minimum, quartile, or median), or calculated the histogram values in limited number of MRI slices,[2,11,13] in the current study, a wide range of voxel-wise ADC histogram values extracted from the whole volume of each tumor solid component were determined and analyzed. In addition, instead of applying arbitrary age cutoffs to differentiate tumors in adult versus pediatric subgroups, we included patients' age as a covariate in our analysis, and focused on tumor localization to cerebellar hemisphere as an objective category. We also devised a stepwise diagnostic algorithm for pretreatment differentiation of cerebellar hemisphere tumors combining ADC histogram values and structural MRI features, which can potentially aid in surgical planning and patient triage for (neo)adjuvant therapy.

Methods

Patients' Characteristics

We retrospectively reviewed the clinical and imaging records of all consecutive patients with pathologically proven diagnosis of cerebellar hemisphere neoplasm at our institution between January 2004 and December 2015. The inclusion criteria were (1) the main lesion localized to the cerebellar hemisphere, (2) surgical pathology diagnosis of a neoplasm (listed in Table 1), and (3) at least one pretreatment MRI with ADC map, T2-weighted, fluid-attenuated inversion recovery (FLAIR), and postcontrast T1-weighted sequences. The exclusion criteria were pathological diagnosis other than a neoplastic process (eg, tumefactive multiple sclerosis, cavernoma), nondiagnostic quality of MRI sequences, and an ADC map quality precluding histogram analysis. The Institutional Review Board approval was obtained, and a waiver of informed consent was provided given the retrospective nature of this study.

MRI Technique

The pretreatment MRI was performed on 1.5 Tesla or 3 Tesla clinical MR scanners using surgical navigation imaging protocol. In majority of patients, spin-echo echo-planar DWI was performed in the 2D axial plane on the GE Discovery MR750 3 Tesla scanner (Waukesha, WI, USA), with image acquisition at b = 0 s/mm^2 and b = 1,000 s/mm^2. Other parameters were: time to repeat = 8,300 ms, echo time = 65 ms, section thickness = 2 mm, field-of-view of 250 mm, and matrix size of 128 × 128. On the 1.5 Tesla GE Signa HD scanner (Waukesha, WI, USA), spin-echo echo-planar DWI was performed in the 2D axial plane with image acquisition at b = 0 s/mm^2 and b = 1,000 s/mm^2. Other parameters were: time to repeat = 9,500 ms, echo time = 90 ms, section thickness = 2 mm, field-of-view of 250 mm, and matrix size of 128 × 128.

Image Analysis for Cerebellar Tumors

A junior staff neuroradiologist (S.P.)–with 6-year experience in brain MRI interpretation and blinded to pathological diagnosis of tumors–reviewed all MRI studies, and determined the imaging features of the main cerebellar hemisphere lesion (listed in Tables 2–7). These features were then corroborated with official clinical reports, and in case of discrepancy or in the absence of critical descriptions in the official report, a senior neuroradiologist (S.C.), with over 20 years of experience in brain tumor imaging, reviewed scans to reach consensus. The lesion texture was categorized as predominantly solid (>80% solid component), mixed solid and cystic, cystic (>80%) with smooth mural nodule, and cystic/necrotic (>80%) with irregular wall. The enhancement pattern of solid component was categorized as homogenous, heterogeneous, or no enhancement. Multiple lesions were considered in patients with discrete distant additional sites of supra- or infratentorial tumoral involvement. The leptomeningeal seeding was defined by the presence of leptomeningeal nodularity and enhancement. The presence of prominent vascular flow voids was determined on T2-weighted images and confirmed on postcontrast T1 series. On visual inspection of the tumor, the solid component would be determined as "T2 hyperintense" if it showed T2 signal higher than the gray matter.[15] This dichotomization is based on the article by Arai et al, which reported that T2 hyperintense signal characteristics of tumor solid component could differentiate pilocytic astrocytomas from medulloblastomas.[15] The maximum thickness of the nonmass-like FLAIR hyperintensity around the main lesion was measured on axial FLAIR images. For calculation of tumor volumes, the main lesions–including both solid and cystic components–were manually segmented on postcontrast T1 images with attention to T2 series for nonenhancing tumor component.

ADC Histogram Analysis

We used the GE Advantage Workstation (GE Healthcare, Milwaukee, WI, USA) for tumor segmentation and ADC histogram analysis. The solid component of the tumors on ADC maps were manually segmented with attention to the postcontrast T1-weighted as well as T2-weighted images, including both enhancing and nonenhancing components. The ADC values were normalized based on the average ADC of cerebrospinal fluid (CSF) in lateral ventricles. Then, we determined the volumetric voxel-wise ADC histogram of the solid component

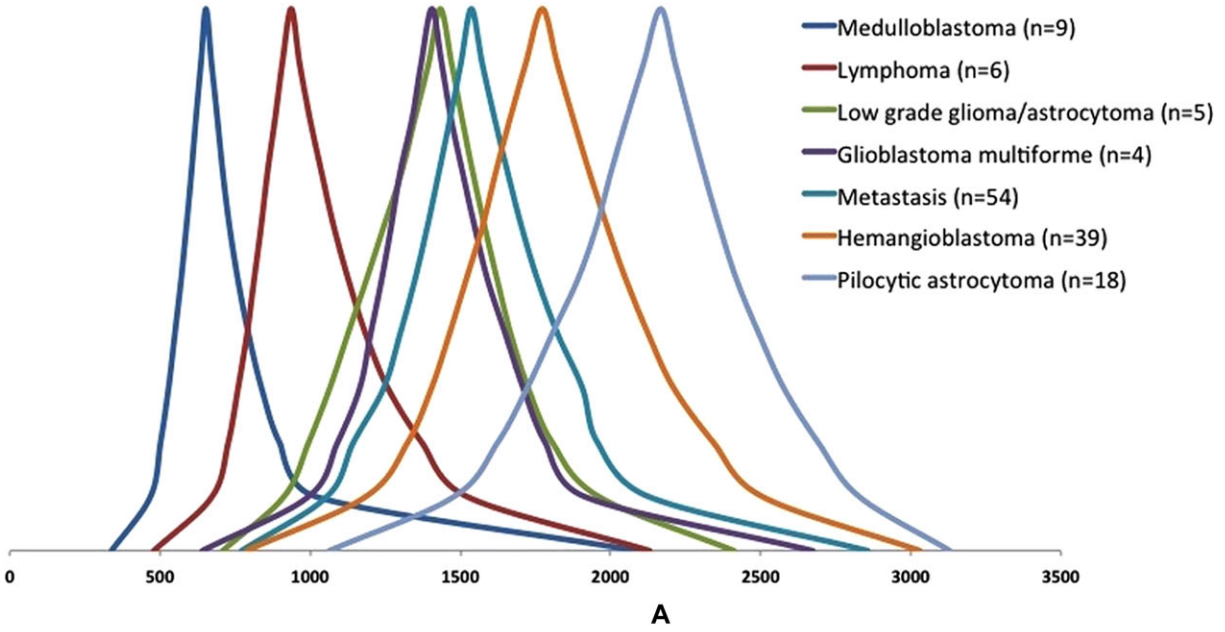

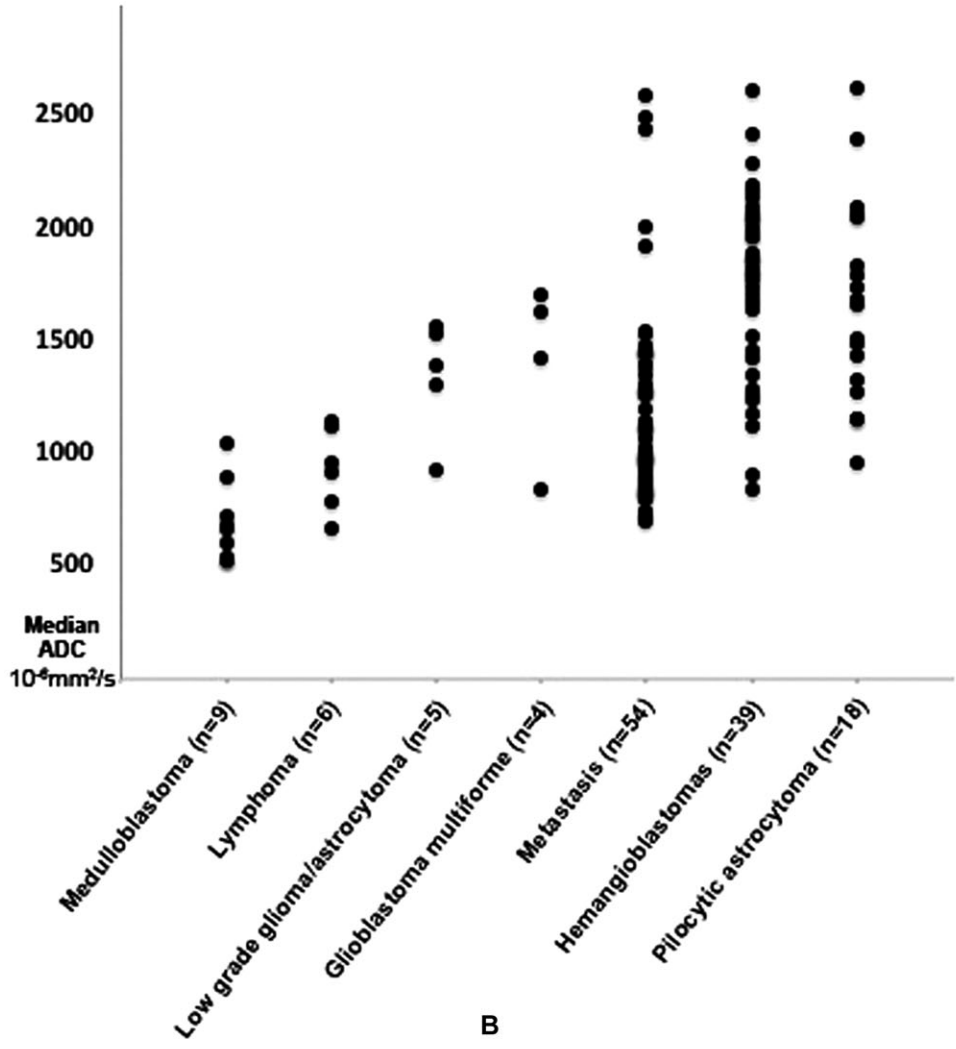

Fig 1. (a) The schematic representation of averaged apparent diffusion coefficient (ADC) histogram distribution among different cerebellar hemisphere tumors. The averaged percentile values among different tumor types are calculated, and representative averaged histograms are modified with the median values depicted at similar height. (b) The distribution of median volumetric voxel-wise apparent diffusion coefficient (ADC) values of the solid component among different cerebellar hemisphere tumors.

Table 2. Clinical Characteristics of Patients Tabulated Based on Cerebellar Hemisphere Tumor Types

	MET ($n = 54$)	HB ($n = 39$)	PA ($n = 18$)	MB ($n = 9$)	LYM ($n = 6$)	LGG ($n = 5$)	GBM ($n = 4$)	*P*-value
Age[a]	57.3 (48.5-66)	46.2 (32.6-68)	20.3 (10.4-27.2)	28.7 (24.2-50.3)	66.4 (51.6-75.1)	40.4 (15.5-68.5)	39.5 (13.1-61.3)	<.001[b]
Gender (male)	18 (33%)	19 (49%)	11 (61%)	2 (22%)	3 (50%)	2 (40%)	1 (25%)	.304

GBM = glioblastoma multiforme; HB = hemangioblastoma; MB = medulloblastoma; MET = metastasis; LGG = low grade glioma/astrocytoma; LYM = lymphoma; PA = pilocytic astrocytoma.
[a]Median age in years (interquartile).
[b]$P < .001$.

Table 3. Different Lesion Textures among Cerebellar Hemisphere Tumors

	MET ($n = 54$)	HB ($n = 39$)	PA ($n = 18$)	MB ($n = 9$)	LYM ($n = 6$)	LGG ($n = 5$)	GBM ($n = 4$)	*P*-value
Predominantly solid (>80%)	39 (72%)	5 (13%)	3 (17%)	6 (67%)	6 (100%)	2 (40%)	2 (50%)	<.001[a]
Mixed solid and cystic	6 (11%)	10 (26%)	7 (39%)	3 (33%)	0 (0%)	3 (60%)	1 (25%)	.036[b]
Cystic (>80%) with mural nodule	3 (6%)	24 (62%)	8 (44%)	0 (0%)	0 (0%)	0 (0%)	0 (0%)	<.001[a]
Cystic/necrotic with irregular wall	6 (11%)	0 (0%)	0 (0%)	0 (0%)	0 (0%)	0 (0%)	1 (25%)	.081

GBM = glioblastoma multiforme; HB = hemangioblastoma; MB = medulloblastoma; MET = metastasis; LGG = low grade glioma/astrocytoma; LYM = lymphoma; PA = pilocytic astrocytoma.
[a]$P < .001$.
[b]$P < .05$.

Table 4. Enhancement Pattern of the Cerebellar Hemisphere Tumor Solid Components

	MET ($n = 54$)	HB ($n = 39$)	PA ($n = 18$)	MB ($n = 9$)	LYM ($n = 6$)	LGG ($n = 5$)	GBM ($n = 4$)	*P*-value
Homogenous enhancement	13 (24%)	36 (92%)	5 (28%)	1 (11%)	4 (67%)	0 (0%)	0 (0%)	<.001[a]
Heterogeneous enhancement	41 (76%)	3 (8%)	13 (72%)	7 (78%)	2 (33%)	4 (80%)	3 (75%)	<.001[a]

GBM = glioblastoma multiforme; HB = hemangioblastoma; MB = medulloblastoma; MET = metastasis; LGG = low grade glioma/astrocytoma; LYM = lymphoma; PA = pilocytic astrocytoma.
[a]$P < .001$.

Table 5. Imaging Characteristics of the Cerebellar Hemisphere Tumors on T2-Weighted and Fluid-Attenuated Inversion Recovery (FLAIR) Sequences

	MET ($n = 54$)	HB ($n = 39$)	PA ($n = 18$)	MB ($n = 9$)	LYM ($n = 6$)	LGG ($n = 5$)	GBM ($n = 4$)	*P*-value
Surrounding FLAIR thickness (mm)	20 (14-28)	17 (10-24)	5 (0-8.5)	10 (5.5-14)	18.5 (15-25.3)	5.5 (3.5-7)	7 (2.5-11)	<.001*
T2 hyperintense solid component	3 (7%)	14 (36%)	12 (67%)	2 (22%)	1 (17%)	5 (100%)	1 (25%)	<.001*
Prominent vascular flow voids	2 (4%)	21 (54%)	0 (0%)	0 (0%)	0 (0%)	0 (0%)	0 (0%)	<.001*

GBM = glioblastoma multiforme; HB = hemangioblastoma; MB = medulloblastoma; MET = metastasis; LGG = low grade glioma/astrocytoma; LYM = lymphoma; PA = pilocytic astrocytoma.
**$P < .001$.

Table 6. Cerebellar Hemisphere Tumors Volume and Rate of Hydrocephalus

	MET ($n = 54$)	HB ($n = 39$)	PA ($n = 18$)	MB ($n = 9$)	LYM ($n = 6$)	LGG ($n = 5$)	GBM ($n = 4$)	*P*-value
Volume (mL)	8.9 (6-17.5)	17.9 (9-28.8)	13.8 (4-42.7)	23.3 (13.8-26.7)	8.9 (6-17.5)	11.9 (7.4-22.1)	11.8 (4.9-24.1)	.034[a]
Hydrocephalus	19 (35%)	19 (49%)	8 (44%)	5 (56%)	2 (33%)	2 (40%)	1 (25%)	.791

GBM = glioblastoma multiforme; HB = hemangioblastoma; MB = medulloblastoma; MET = metastasis; LGG = low grade glioma/astrocytoma; LYM = lymphoma; PA = pilocytic astrocytoma.
[a]$P < .05$.

and calculated percentile values with 5 percentile increment gaps for statistical analysis (ie, minimum, 5th, 10th, 15th percentile, ….). The ADC mean, histogram kurtosis, and skewness values were also determined. The schematic averaged ADC histograms of different tumor types were developed for visual comparison (Fig 1a), where the average histogram percentile values were calculated among patients with each tumor type, and resultant averaged histograms were modified so that median values would have the same height.

Statistical Analysis

The data are presented as median (interquartile) and frequency (percentage), for continuous and nominal variables, respectively. We applied the ANOVA with Tukey's post hoc analysis to compare continuous variables between different tumor types. For comparing the frequency of nominal variables among different tumor types, we applied the χ^2 test. The nonparametric Kruskal–Wallis and Mann–Whitney U tests were applied for

Table 7. Multiplicity and Localization of the Cerebellar Hemisphere Tumors

	MET ($n = 54$)	HB ($n = 39$)	PA ($n = 18$)	MB ($n = 9$)	LYM ($n = 6$)	LGG ($n = 5$)	GBM ($n = 4$)	*P*-value
Multiple lesions	16 (%)	4 (10%)	1 (6%)	2 (22%)	1 (17%)	1 (20%)	2 (50%)	.120
Leptomeningeal extension	4 (7%)	0 (0%)	0 (0%)	0 (0%)	0 (0%)	1 (20%)	1 (25%)	.080
Cerebellar peduncle involvement	4 (7%)	6 (15%)	2 (11%)	4 (44%)	1 (17%)	2 (40%)	3 (75%)	.002[a]

GBM = glioblastoma multiforme; HB = hemangioblastoma; MB = medulloblastoma; MET = metastasis; LGG = low grade glioma/astrocytoma; LYM = lymphoma; PA = pilocytic astrocytoma.
[a] $P < .01$.

comparison of ADC percentile values among different tumor types. Separate binary logistic regression analyses were performed to identify the independent predictors for each type of cerebellar hemisphere tumors. The continuous variables were dichotomized based on operating point values on the receiver operating characteristics (ROC) curve analysis. The ROC curve operating points were selected so the classifier had the maximum sum of sensitivity and specificity. The test characteristics including area under the curve (AUC), sensitivity, specificity, positive predictive value (PPV), and negative predictive value (NPV) are expressed as ratio (95% confidence interval). All statistical analyses were performed using the statistics software SPSS 22.0 (IBM, Somers, NY, USA).

Results

Patients

A total of 142 patients met the inclusion criteria for our study. The median age of patients at the time of diagnosis was 47 (30.4-64.5) years, and ranging from 1 month to 78 years. The most common histologic tumor types were metastasis, hemangioblastoma, pilocytic astrocytoma, and medulloblastoma (Table 1). The MRI scans of 108 (76%) patients were obtained with 3 Tesla scanners; and 34 (24%) were scanned with 1.5 Tesla machines.

ADC Histogram Analysis

Figure 1(a) demonstrates the schematic representation of averaged ADC percentile values among different cerebellar hemisphere tumors. Overall, medulloblastomas had the lowest and pilocytic astrocytomas had the highest ADC values. Figure 1(b) demonstrates the distribution of median ADC values among different cerebellar hemisphere tumors. Using the Kruskal–Wallis test, there was significant difference in ADC percentile values, skewness, and kurtosis between different tumor types. In separate univariate analyses among different types of cerebellar hemispheric tumor, medulloblastomas had significantly lower ADC histogram percentile values compared to others (Fig 2). Hemangioblastomas and pilocytic astrocytomas also had higher ADC percentile values compared to lymphomas and metastases (Fig 2). Comparing patients with the two most common cerebellar hemisphere tumors–namely, metastasis ($n = 54$, 38%) and hemangioblastoma ($n = 39$, 27.5%)–hemangioblastomas had significantly higher ADC values (Fig 2); and an ADC 90th percentile could optimally differentiate these two tumors from each other with a ROC AUC of .82 (.74-.91, $P \leq .001$). An ADC 90th percentile $> 2{,}000 \times 10^{-6}$ mm^2/s could differentiate hemangioblastomas from metastases with 80% (63%-90%) sensitivity, 87% (74%-94%) specificity, 82% (65%-92%) PPV, and 85% (73%-93%) NPV.

Structural Imaging Characteristics of Cerebellar Hemisphere Tumors

Tables 2–7 summarize the univariate comparison analysis of imaging characteristics between different types of cerebellar hemisphere tumors.

There was a significant difference in average age of patients based on each histologic tumor type (Table 2, $P < .001$). On post hoc analysis, patients with pilocytic astrocytoma were significantly younger compared to those with hemangioblastoma ($P < .001$), metastasis ($P < .001$), and lymphoma ($P < .001$). Also, patients with medulloblastoma were significantly younger compared to those with metastasis ($P = .003$), and lymphoma ($P = .012$). There was no significant difference in gender ratio among various tumor types.

There was also significant difference in tumor textures (Table 3). Specifically, while all lymphomas (100%), and majority of metastases (72%), and medulloblastomas (67%) were predominantly solid ($P < .001$), the pilocytic astrocytomas and hemangioblastomas demonstrated mixed solid-and-cystic ($P = .036$), or cystic with smooth mural nodularity ($P < .001$). There was no significant difference in ratio of tumors with cystic/necrotic texture and irregular wall ($P = .081$).

Regarding the enhancement pattern (Table 4), the majority of hemangioblastomas (92%) and lymphomas (67%) demonstrate homogenous enhancement ($P < .001$); whereas, metastases, pilocytic astrocytomas, medulloblastomas, and GBMs predominantly showed heterogeneous enhancement ($P < .001$).

On FLAIR sequences, there was a significant difference between various tumors with regards to the degree of peritumoral FLAIR hyperintensity (Table 5, $P < .001$). On post hoc analysis, metastases had thicker rind of surrounding FLAIR hyperintensity compared to medulloblastomas ($P = .038$), low-grade glioma/astrocytomas ($P = .016$), and pilocytic astrocytomas ($P < .001$). Hemangioblastomas also had greater thickness of surrounding FLAIR hyperintensity compared to low-grade glioma/astrocytomas ($P = .039$), and pilocytic astrocytomas ($P < .001$). The peritumoral FLAIR hyperintensity surrounding lymphomas was also greater compared to pilocytic astrocytomas ($P = .027$).

All low-grade glioma/astrocytomas and 67% of pilocytic astrocytomas had T2 hyperintense solid components (Table 5, $P < .001$). Prominent vascular flow voids were only found in 21 (54%) hemangioblastomas and 2 (4%) metastases (Table 5, $P < .001$).

Regarding the tumor size (Table 6), pilocytic astrocytomas had significantly larger volumes compared to metastases on post hoc analysis ($P = .014$). However, there was no significant difference in rate of hydrocephalus (Table 6).

Imaging evidence of tumor infiltration into cerebellar peduncles was seen in 75% of GBMs, 44% of medulloblastomas,

Fig 2. Comparison of different apparent diffusion coefficient (ADC) histogram values between cerebellar hemisphere tumors. The *P*-values for separate Mann–Whitney U tests are reported; and *P*-values < .05 are color coded with orange and red. GBM = glioblastoma multiforme; HB = hemangioblastoma; MB = medulloblastoma; MET = metastasis; LGG = low grade glioma/astrocytoma; LYM = lymphoma; PA = pilocytic astrocytoma.

and 40% of low-grade glioma/astrocytoma (Table 7); whereas the rates of cerebellar peduncle involvement were less than 20% among other tumors ($P = .002$). The presence of multiple lesions and leptomeningeal seeding were not significantly different among different types of cerebellar hemispheric tumors (Table 7).

Differentiation of the Cerebellar Hemisphere Tumors by Imaging

Applying separate binary logistic regressions, we developed a stepwise diagnostic algorithm for differentiation of cerebellar hemisphere tumors (Fig 3). A 15th percentile ADC value ($P < .001$) was an independent predictor of medulloblastomas (Figs 3 and 4). Using the ROC analysis, an ADC 15th percentile $< 580 \times 10^{-6}$ mm^2/s could differentiate medulloblastomas from other cerebellar tumors with ROC AUC of .98 (.95-1.00, $P < .001$).

The homogenous enhancement pattern ($P < .001$), presence of prominent vascular flow voids on T2-weighted images ($P = .001$), cystic appearance with mural nodularity ($P < .001$), and mixed solid-cystic texture patterns ($P = .004$) were independent predictors of hemangioblastomas (Figs 3 and 4).

The patients' age ($P = .001$), T2 hyperintensity of solid component ($P = .049$), presence of enhancement ($P = .046$), and mural nodule texture pattern ($P = .046$) were independent predictors of pilocytic astrocytomas (Figs 3 and 4). Notably, 17/18 patients with pilocytic astrocytoma were younger than 40 years.

The heterogeneous enhancement pattern ($P < .001$), surrounding FLAIR hyperintensity thickness ($P = .001$), multiplicity of lesions ($P = .011$), solid appearance ($P < .001$), and cystic/necrotic center with irregular border texture patterns ($P < .004$) were independent predictors of metastasis (Figs 3 and 4).

It should be noted that all lymphomas had a 15th percentile ADC value $< 950 \times 10^{-6}$ mm^2/s, although such a characteristic could not differentiate lymphomas from (hypercellular) metastatic lesions (Figs 2 and 3).

Discussion

Our results show how the ADC histogram analysis can be applied for differentiation of cerebellar hemisphere tumors on pretreatment MRI, with medulloblastomas and pilocytic astrocytoma having the lowest, and the highest ADC histogram values, respectively. In particular, differentiation of the two most common cerebellar hemisphere tumors–metastases and hemangioblastomas–can be challenging based on qualitative structural imaging alone. Both metastases and hemangioblastomas affect adult patient population, localize to cerebellar hemisphere, present with enhancing components, and tend to have prominent surrounding FLAIR hyperintensity (Tables 2–5). The ADC histogram analysis can help differentiate these two adult cerebellar hemisphere tumors, with hemangioblastomas showing higher ADC histogram values compared to metastases. Also, the combination of ADC histogram

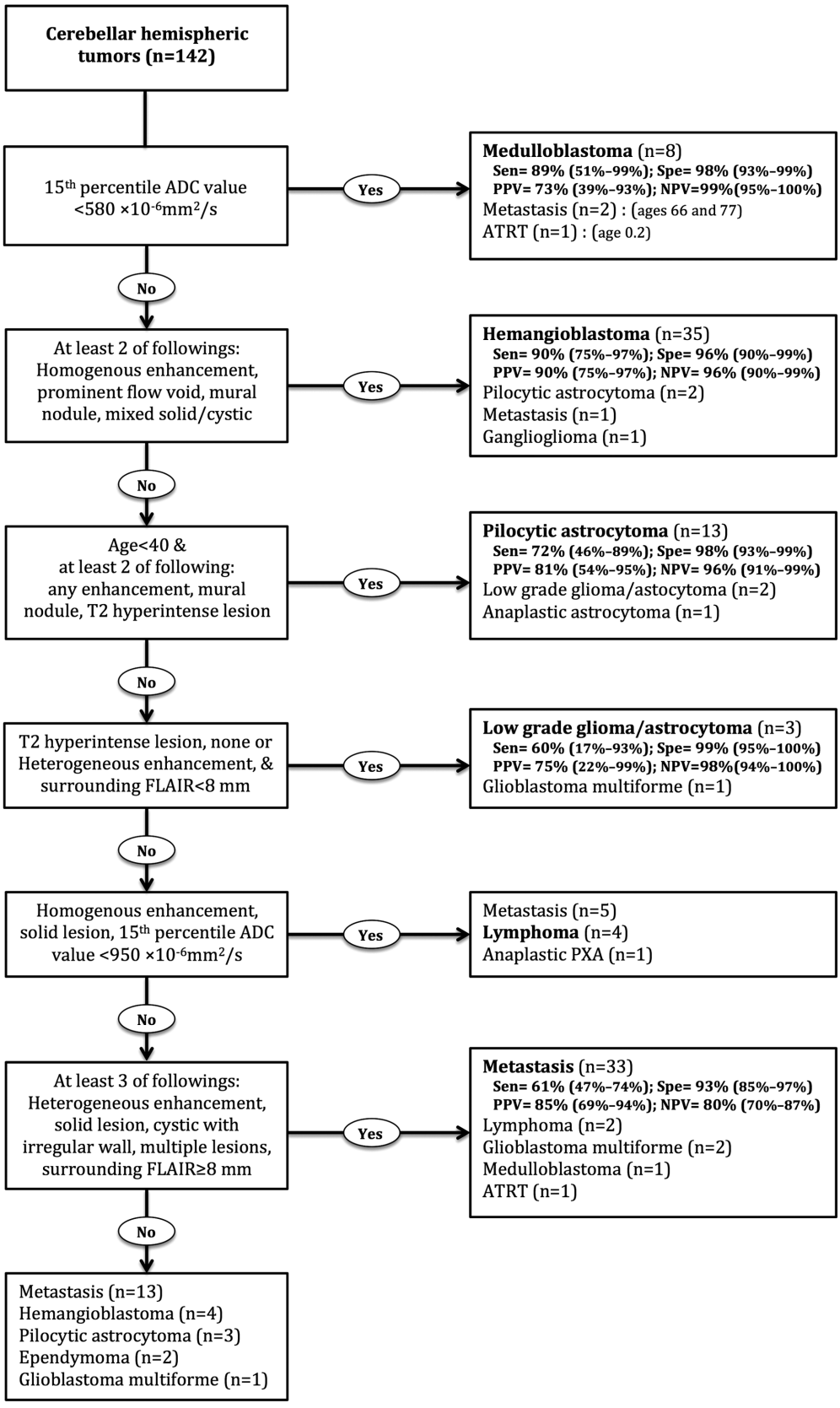

Fig 3. Diagnostic algorithm for differentiation of cerebellar hemisphere tumors. ADC = apparent diffusion coefficient; ATRT = atypical teratoid/rhabdoid tumor; FLAIR = fluid-attenuated inversion recovery; NPV = negative predictive value; PXA = pleomorphic xanthoastrocytoma; PPV = positive predictive value; Sen = sensitivity; Spe = specificity.

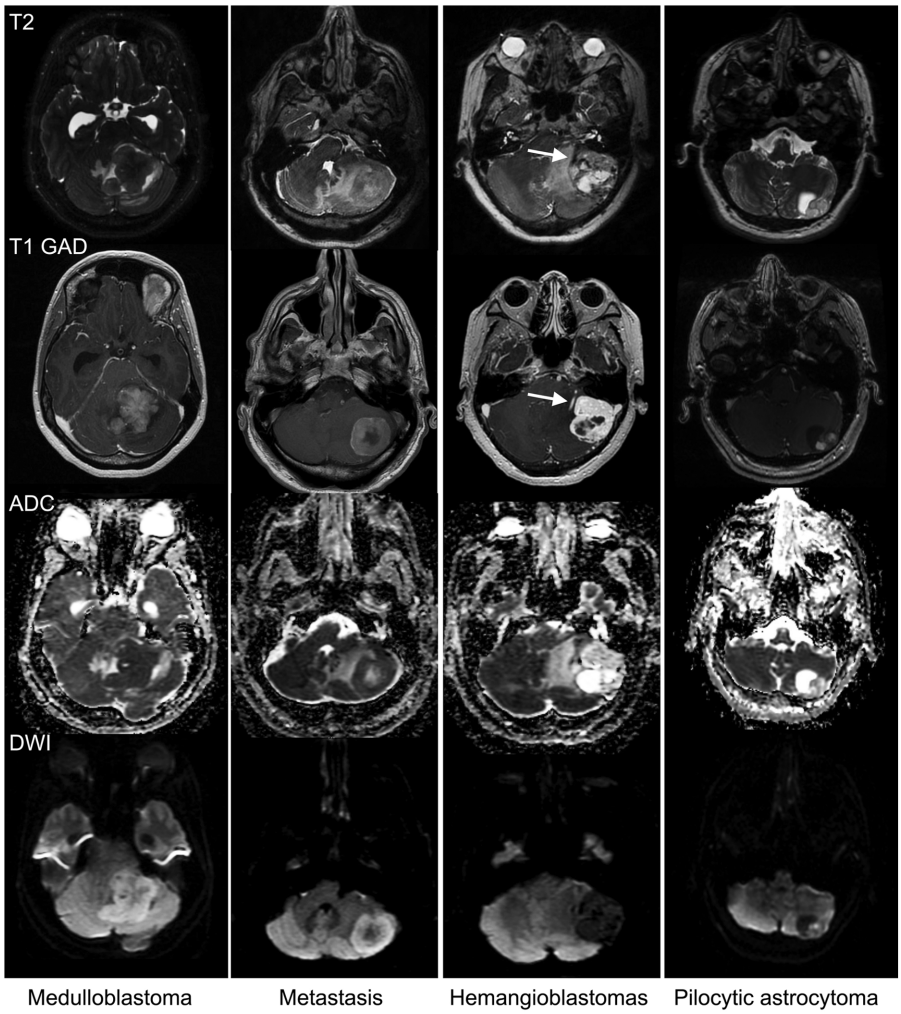

Fig 4. From top to bottom row, T2-weighted, postgadolinium-based contrast T1-weighted (T1 GAD), apparent diffusion coefficient (ADC), and diffusion-weighted imaging (DWI) series among representative patients with medulloblastoma, metastasis, hemangioblastoma, and pilocytic astrocytoma (left to right column). The medulloblastoma was found in a 53-year-old man presented with a heterogeneously enhancing left cerebellar mass showing reduced diffusion—ADC 15th percentile value of 486 $\times$ 10^{-6} mm^2/s. The metastasis was found in a 59-year-old man presented with a heterogeneously enhancing left cerebellar mass and moderate surrounding T2 hyperintensity—ADC 90th percentile value of 1,345 $\times$ 10^{-6} mm^2/s. The hemangioblastoma was found in a 68-year-old woman presented with an avidly enhancing partially cystic left cerebellar mass, moderate surrounding T2 hyperintensity, and prominent vascular flow voids on T2 and postcontrast images (arrows). The ADC 90th percentile value was 2,456 $\times$ 10^{-6} mm^2/s. The pilocytic astrocytoma was found in a 15-year-old boy presented with a cystic left cerebellar mass, a T2 hyperintense solid nodule, and high diffusibility on ADC map.

variables, patients' age, and other structural imaging features on pretreatment MRI (ie, lesion texture, enhancement pattern, presence of prominent vascular flow voids, surrounding FLAIR hyperintensity, and solid component T2 hyperintensity) could be applied to develop an objective diagnostic algorithm for differentiation of cerebellar hemisphere tumors (Fig 3).

In the present study, we included all consecutive patients with cerebellar hemisphere tumors, which is a distinction from prior literature restricting their study cohorts based on patients' age, or with selective inclusion of certain tumor subtypes.[2,9–11,16] Moreover, we determined the volumetric voxel-wise ADC histogram profile of tumors rather than examining limited 2D region-of-interest measurements.[2,9,11,13] Also, instead of limiting our analysis to specific histogram variables such as minimum, median, or quartile ADC values, we analyzed different histogram percentile variables between tumor types.[2,9,11,13] Eventually, along with volumetric ADC histogram variables, different imaging features and patient's age were evaluated to develop a multivariate diagnostic algorithm for differentiation of cerebellar hemisphere tumors on pretreatment MRI in consecutive patient population.

As stated above, metastases and hemangioblastomas were the most common cerebellar hemisphere tumors in our cohort (Table 1). Comparing these two tumor types with each other, an ADC 90th percentile $>$ 2,000 $\times$ 10^{-6} mm^2/s could differentiate hemangioblastomas from cerebellar metastases with 82% accuracy (95% confidence interval: 74%-91%). Thus, when the differential diagnosis of a cerebellar hemisphere tumor is narrowed down to hemangioblastoma versus metastasis, the ADC histogram profile analysis can provide quantitative measures for differentiation. Notably, a recent study suggested that using a high b value DWI sequence (b-value of 4,000 instead of 1,000) could better differentiation posterior cranial fossa hemangioblastomas from metastases based on the ADC ratio

value of lesion and normal appearing tissue.[17] Among our consecutive patients with cerebellar hemisphere tumors, however, imaging characteristics such as enhancement pattern, tumor texture, presence of prominent vessel void, surrounding FLAIR hyperintensity, and multiplicity of lesions were also helpful in the distinction of hemangioblastomas from metastases (Figs 3 and 4).

Pilocytic astrocytomas and medulloblastomas are the most common primary neoplasms of the posterior cranial fossa in children.[8,18] On cellular level, pilocytic astrocytomas are characterized by an abundant myxoid stroma.[7] Subsequently, these tumors are associated with high diffusibility on ADC maps.[7] In current series, pilocytic astrocytomas demonstrate the highest ADC histogram values among cerebellar hemisphere tumors, consistent with prior reports.[2,9,11] In multivariate diagnostic algorithm among consecutive patients, the age, solid component T2 hyperintensity, mural nodularity, and presence of enhancement could best differentiate the pilocytic astrocytomas from other cerebellar hemisphere tumors (Fig 3). Arai et al have also shown that the majority of pilocytic astrocytomas demonstrate solid component T2 hyperintensity, with a signal similar to CSF or higher than gray matter.[15]

Histologically, medulloblastomas are highly cellular tumors comprised of small round blue cells with reduced diffusion on DWI.[7] Using the support vector machine classification analysis in 40 children with posterior cranial fossa ependymoma, medulloblastoma, and pilocytic astrocytoma, Rodriguez Gutierrez et al reported that combination of ADC histogram 25th percentile, 75th percentile, and skewness values can identify medulloblastomas with 95.8% overall accuracy.[9] However, lesion location was not specified or analyzed in their study.[9] In the current study, we found that an ADC 15th percentile value $< 580 \times 10^{-6}$ mm^2/s could identify cerebellar hemisphere medulloblastomas with an overall accuracy of 98% (Figs 3 and 4). These results confirm that ADC histogram analysis can provide an objective measure to help with differentiation of medulloblastomas among consecutive cerebellar hemisphere tumors.[2,11]

Notably, the average age of patients with medulloblastoma in our cohort was 34.9 years. There were 3 false positive cases classified as medulloblastoma based on the histogram cutoff of ADC 15th percentile value $< 580 \times 10^{-6}$ mm^2/s. These include 66- and 77-year-old patients with metastases, and a 2-month-old infant with atypical teratoid rhabdoid tumor (ATRT), suggesting that patients' age can help with differentiation of cerebellar hemisphere medulloblastomas from highly cellular metastases and ATRTs.

Recent genomic studies of medulloblastomas have identified four distinct molecular subgroups (wingless, sonic hedgehog, group 3, and group 4) as predictive of clinical outcome.[19] Perreault et al have shown that the location and enhancement pattern of medulloblastomas were the only imaging features distinguishing different molecular subtypes.[6] They found that wingless medulloblastomas were mostly centered in cerebellar peduncles, sonic hedgehog tumors predominantly involved cerebellar hemispheres, and groups 3 and 4 were mainly in midline protruding into the fourth ventricle.[6] Unfortunately in our cohort, the molecular subtype was only available in 4 medulloblastomas, all of which were sonic hedgehog. Future studies will hopefully illuminate whether the ADC histogram can help with differentiation of molecular genetic subtypes of medulloblastomas.

Some prior studies have applied curve-fitting models to identify and evaluate multimodal ADC histogram portfolio of brain tumors–specifically GBM.[14] Pope et al have identified bimodal distribution of ADC histogram within the contrast-enhancing component of GBMs, and applied such models for prognostication of Bevacizumab-treated GBMs.[14] On the other hand, Rahman et al found that a four-modal Gaussian function curve-fitting algorithm improved the accuracy and reproducibility of ADC histogram fitting in both enhancing and nonenhancing T2 hyperintense components of GBM.[20] On the contrary, Zolal et al reported an approximately normal, unimodal distribution of the ADC histogram in many of GBMs, "making a two normal distribution mixture curve analysis meaningless."[21] In a study of children with diffuse intrinsic pontine glioma, Poussaint et al found that 46 patients had a unimodal ADC histogram peak within the enhancing component, and 9 had bimodal peaks.[13] Given the conflicting prior reports and based on our visual assessment of ADC histograms, all histogram values in the current study were calculated based on a unimodal distribution assumption.

Other limitations of our study include retrospective design and relatively small numbers of some tumor types. Moreover, the inclusion criteria for this study limit the subjects to those with known cerebellar hemispheric neoplasm; whereas in real-world clinical practice, nonneoplastic tumor-mimics should be differentiated from tumors. Thus, the test characteristics in differentiation algorithm depicted in Figure 3 may not reflect the results in realistic clinical practice population. In addition, patients have been scanned over an 11-year period, which adds to the heterogeneity of data. There may also be some inherent variability in manual segmentation of tumor solid components, which can potentially limit the reproducibility of our findings.

In conclusions, the ADC histogram analysis can help in pretreatment imaging differentiation of cerebellar hemisphere tumors, particularly metastasis, hemangioblastomas, and medulloblastomas. This is especially helpful since the differentiation of metastasis and hemangioblastomas (the two most common adult cerebellar tumors) may be challenging solely based on structural MRI features. A combination of ADC histogram analysis and structural imaging features can offer a useful diagnostic algorithm for semiquantitative and objective differentiation of cerebellar hemisphere tumors, which can potentially improve surgical planning and guide early therapeutic strategy.

References

1. Koral K, Zhang S, Gargan L, et al. Diffusion mri improves the accuracy of preoperative diagnosis of common pediatric cerebellar tumors among reviewers with different experience levels. AJNR Am J Neuroradiol 2013;34:2360-5.
2. Pierce T, Kranz PG, Roth C, et al. Use of apparent diffusion coefficient values for diagnosis of pediatric posterior fossa tumors. Neuroradiol J 2014;27:233-44.
3. Kang KM, Sohn CH, You SH, et al. Added value of arterial spin-labeling mr imaging for the differentiation of cerebellar hemangioblastoma from metastasis. AJNR Am J Neuroradiol 2017;38:2052-8.
4. Harreld JH, Hwang SN, Qaddoumi I, et al. Relative adc and location differ between posterior fossa pilocytic astrocytomas with and without gangliocytic differentiation. AJNR Am J Neuroradiol 2016;37:2370-5.

5. Keil VC, Warmuth-Metz M, Reh C, et al. Imaging biomarkers for adult medulloblastomas: Genetic entities may be identified by their mr imaging radiophenotype. AJNR Am J Neuroradiol 2017;38:1892-8.
6. Perreault S, Ramaswamy V, Achrol AS, et al. Mri surrogates for molecular subgroups of medulloblastoma. AJNR Am J Neuroradiol 2014;35:1263-9.
7. Rumboldt Z, Camacho DL, Lake D, Welsh CT, Castillo M. Apparent diffusion coefficients for differentiation of cerebellar tumors in children. AJNR Am J Neuroradiol 2006;27:1362-9.
8. Jaremko JL, Jans LB, Coleman LT, Ditchfield MR. Value and limitations of diffusion-weighted imaging in grading and diagnosis of pediatric posterior fossa tumors. AJNR Am J Neuroradiol 2010;31:1613-6.
9. Rodriguez Gutierrez D, Awwad A, Meijer L, et al. Metrics and textural features of mri diffusion to improve classification of pediatric posterior fossa tumors. AJNR Am J Neuroradiol 2014;35:1009-15.
10. Bull JG, Saunders DE, Clark CA. Discrimination of paediatric brain tumours using apparent diffusion coefficient histograms. Eur Radiol 2012;22:447-57.
11. Pierce TT, Provenzale JM. Evaluation of apparent diffusion coefficient thresholds for diagnosis of medulloblastoma using diffusion-weighted imaging. Neuroradiol J 2014;27:63-74.
12. Kralik SF, Taha A, Kamer AP, et al. Diffusion imaging for tumor grading of supratentorial brain tumors in the first year of life. AJNR Am J Neuroradiol 2014;35:815-23.
13. Poussaint TY, Vajapeyam S, Ricci KI, et al. Apparent diffusion coefficient histogram metrics correlate with survival in diffuse intrinsic pontine glioma: a report from the pediatric brain tumor consortium. Neuro Oncol 2016;18:725-34.
14. Pope WB, Qiao XJ, Kim HJ, et al. Apparent diffusion coefficient histogram analysis stratifies progression-free and overall survival in patients with recurrent gbm treated with bevacizumab: a multicenter study. J Neurooncol 2012;108:491-8.
15. Arai K, Sato N, Aoki J, et al. Mr signal of the solid portion of pilocytic astrocytoma on t2-weighted images: is it useful for differentiation from medulloblastoma? Neuroradiology 2006;48:233-7.
16. Cha J, Kim ST, Nam DH, et al. Differentiation of hemangioblastoma from metastatic brain tumor using dynamic contrast-enhanced mr imaging. Clin Neuroradiol 2017;27:329-34.
17. Onishi S, Hirose T, Takayasu T, et al. Advantage of high b value diffusion-weighted imaging for differentiation of hemangioblastoma from brain metastases in posterior fossa. World Neurosurg 2017;101:643-50.
18. Yeom KW, Mitchell LA, Lober RM, et al. Arterial spin-labeled perfusion of pediatric brain tumors. AJNR Am J Neuroradiol 2014;35:395-401.
19. Northcott PA, Korshunov A, Witt H, et al. Medulloblastoma comprises four distinct molecular variants. J Clin Oncol 2011;29:1408-14.
20. Rahman R, Hamdan A, Zweifler R, et al. Histogram analysis of apparent diffusion coefficient within enhancing and nonenhancing tumor volumes in recurrent glioblastoma patients treated with bevacizumab. J Neurooncol 2014;119:149-58.
21. Zolal A, Juratli TA, Linn J, et al. Enhancing tumor apparent diffusion coefficient histogram skewness stratifies the postoperative survival in recurrent glioblastoma multiforme patients undergoing salvage surgery. J Neurooncol 2016;127:551-7.